

# Active gels: from chemical microreactor to polymeric actuator

Baptiste Blanc,<sup>1</sup> Zhenkun Zhang,<sup>2</sup> Eric Liu,<sup>3</sup> Ning Zhou,<sup>4</sup> Hyunmin Yi,<sup>3</sup> and Seth Fraden<sup>1</sup>

<sup>1</sup>*Department of Physics, Brandeis University, 415 South St., Waltham, MA 02454, United States*

<sup>2</sup>*Key Laboratory of Functional Polymer Materials of Ministry of Education, Institute of Polymer Chemistry, College of Chemistry, Nankai University, 300071 Tianjin, China*

<sup>3</sup>*Department of Chemical and Biological Engineering,*

*Tufts University, Medford, Massachusetts 02155, United States*

<sup>4</sup>*Department of Chemistry, Brandeis University, 415 South St., Waltham, MA 02454, United States*

We report on a new synthesis protocol, experimental characterization and theoretical modeling of Belousov-Zhabotinsky (BZ) hydrogels. BZ gels combine the ability to convert chemical energy into actuation with a sensing capability. Our new two-step synthesis technique allows independent optimization of the chemical and the mechanical properties of BZ gels. We demonstrate that the strain of these BZ gels can be made arbitrarily large by decreasing their bulk modulus, an important result for the design of shape-changing hydrogels. In addition to strain, we argue that the stress developed by BZ gels is a better metric for assessing the utility of a given gel for chemomechanical energy conversion. We highlight the role of the surrounding media for the occurrence of hydrogel oscillation, which is determined by the Damköhler number, the ratio of chemical reaction to diffusion rates. These experimental findings are supported by a Flory-Huggins theory for polyelectrolyte gels coupled to a Vanag-Epstein model of BZ chemistry.

PACS numbers: .

## INTRODUCTION

The existence of living organisms is evidence that functional motile autonomous materials can be built robustly using macromolecules. However, assembling polymers that possess these properties remains an open challenge. Current endeavors in this field can be classified in two main categories. The first one consists in constructing life-like materials from building blocks that are taken from the living realm, for instance proteins [1–3], molecular motors [4–7], and cells [8, 9], or from synthetic molecules and colloidal particles [10] because these elements have the coveted capability of autonomously converting chemical energy into mechanical work. The second one couples passive engineered polymeric materials such as colloids, hydrogels and elastomers to external power sources [11–13]. Although both of these approaches have shown promising applications, the design of synthetic functional chemomechanical materials is in its infancy and could lead to the creation of life-like machines with augmented performance compared to what evolution has created [14].

In this work, we present a synthetic mechanically active hydrogel driven by a chemical oscillator in which the mechanical and chemical properties can be separately optimized. Inspired by Yoshida’s work [15], we create acrylamide hydrogels doped with the catalyst of the Belousov-Zhabotinsky (BZ) reaction [16]. When placed in an aqueous solution containing the ingredients of the BZ reaction, these gels cyclically convert chemical energy into mechanical work. The simplest description of the BZ gel mechanism consists in separating the BZ chemical reaction from its actuation. In the BZ reaction, an autocatalytic activator drives the catalyst to its oxidized state and generates an inhibitor that returns the catalyst to

its reduced state [17]. The cyclic change of the oxidation state of the catalyst induces the oscillatory swelling of the gel.

Over the past 25 years, material scientists have strived to maximize the oscillatory strain amplitude of BZ gels. Controlling strain is crucial for the design of shape changing functional elements, such as bimorphs [18–20]. The composition of the BZ gels [22, 28, 33], the architecture of the catalyst [22, 26], the charge of the monomer [21, 22], the porous structure of the hydrogel [22–25], the shape of the gels [27, 29] and the chemical environment of the gel [30] have been reported to influence the swelling of the BZ gel. Here, we provide experimental and theoretical evidence supporting that the strain of a BZ gel can be made arbitrarily large by decreasing its bulk modulus, elucidating a system-independent mechanism for increasing the strain of active gels.

However, to optimize the properties of an active gel for engineering applications, we argue that it is necessary to characterize both the strain and the stress fields. To understand why, conceptualize the active gel as a spring in which an active force ( $F$ ) drives a displacement ( $x$ ) that is proportional to the passive restoring force of the gel ( $k$ ), e.g.  $F = kx$ . When a BZ gel experiences a large strain, e.g.  $x = F/k$ , upon oxidation of the ruthenium catalyst, one can not distinguish if this is caused by a gel having a low bulk modulus (small  $k$ ) or by a large active stress (large  $F$ ) caused by the oxidation of the catalyst. Measuring the stress and the strain allows one to disentangle the role of the chemical driving forces from the elastic restorative forces of the gel. Therefore the stress, a quantity so far understudied in the field of BZ gels, is of central importance because it directly couples to molecular properties of the polymer [31]. Here we simultaneously measure the gels’ strain and stress and

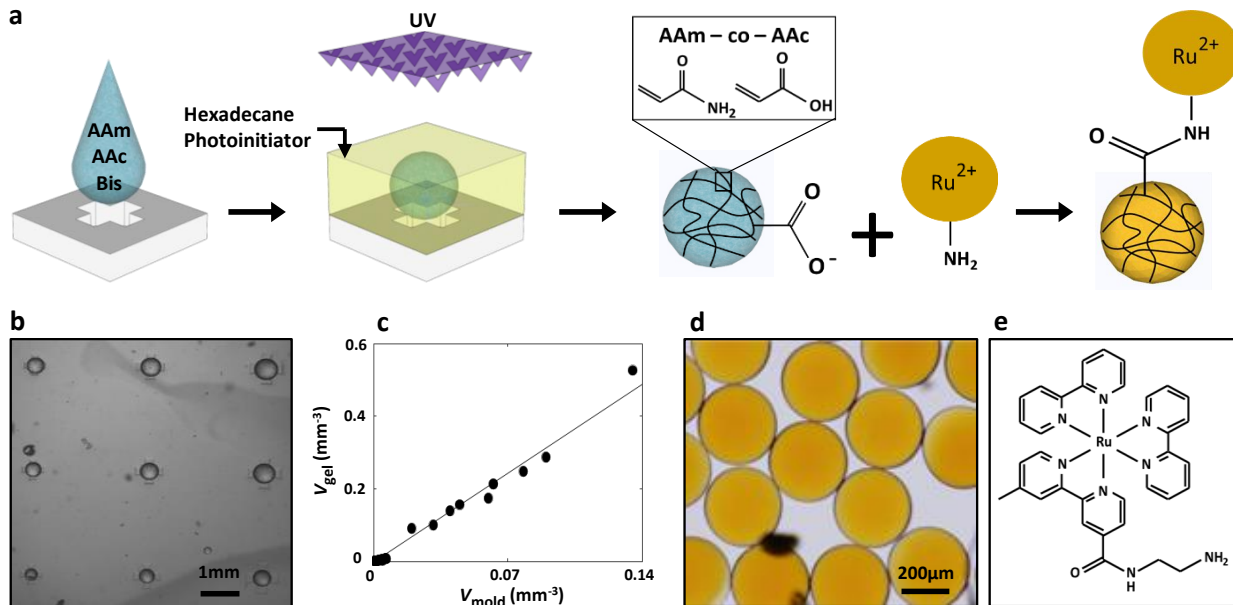


FIG. 1. (a) Schematic of the gel synthesis process. (b) Bright-field image of pre-gel drops on a PDMS mold before UV exposure. The drops are an aqueous solution of 15% acrylamide (AAm), 1.5% acrylic acid (AAc), 1% Bisacrylamide (Bis). The outer solution is hexadecane. (c) Relation between the volume of the micropatterned wells of the PDMS mold and the volume of the crosslinked gel. The line represents the theoretical prediction assuming that the volume of the gel is proportional to the volume of the micropatterned wells of the PDMS. (d) Bright-field image of  $200\mu\text{m}$  diameter gels of composition 15%AAm, 1.5%AAc, 1%Bis coupled with the ruthenium catalyst. (e) Chemical structure of the ruthenium catalyst synthesized in this study: Bis(2,2'-bipyridine)-4'-methyl-4-amido ethylamine-ruthenium bis(hexafluorophosphate), noted  $\text{Ru}(\text{bpy})_2(\text{bpyEtAm})(\text{PF}_6)_2$ .

we demonstrate that varying the catalyst content in the gel allows tuning of the stress.

We also study several out-of-equilibrium properties of oscillating BZ gels and demonstrate experimentally and theoretically that the radius of a spherical gel affects the period of the BZ reaction and even controls whether or not the gel even oscillates. We measured the timescale of BZ gel swelling as a function of radius and demonstrate that the factor limiting the strain amplitude is the diffusive nature of gel swelling, which has a long timescale compared to the shorter period of the BZ oscillation. We finally discuss a simple way to overcome this impediment.

## RESULTS AND DISCUSSION

Spherical BZ hydrogels are fabricated through a two-step process (Figure 1)[33–35]. First, we create a hydrogel by simultaneously polymerizing mixtures of inert and functional monomers in predetermined stoichiometric ratios and crosslinking the polymers together. Second, we attach a pendant BZ catalyst to the functional groups. This two-step process is designed to allow the production of BZ gels with independent control over their mechanical properties, their chemically oscillating behavior and their geometry. The stiffness of the gel can be systematically controlled by varying the cross-link density before introducing the catalyst, while the catalyst concentra-

tion is set by the concentration of functional monomers. Control over the size of the spherical gel is accomplished by combining an emulsion polymerization approach and a molding process [36]. Using this protocol, we created gels from  $100\mu\text{m}$  to  $600\mu\text{m}$  in diameter with a bulk modulus as soft as 10 kPa. Notable desirable features of the two-step process are the ability to homogeneously incorporate the ruthenium trisbipyridine catalyst in the gel and to create gels with a higher catalyst concentration than the solubility limit. Here we report homogeneously incorporating synthesized  $\text{Ru}(\text{bpy})_2(\text{bpyEtAm})(\text{PF}_6)_2$  in the gel with catalyst concentrations up to 12mM, which is significantly higher than the solubility limit in water (Supplementary SM 2, SM 3).

### Optimizing the strain upon oxidation of BZ gels

The strain of a BZ gel is the traditional metric to assess the chemomechanical energy conversion because the mechanical strain energy density depends quadratically on this quantity and because shape changing elements such as bimorphs rely on bending deformations that are controlled by the strain [18]. Therefore, we first investigate the BZ hydrogels' composition that maximizes strain upon oxidation of the ruthenium catalyst. Gels are immersed in oxidative solutions made of sodium bromate and sulfuric acid at concentrations,  $[\text{NaBrO}_3]=0.08\text{M}$

and  $[\text{H}_2\text{SO}_4]=0.4\text{M}$ , for which the ruthenium catalyst is strongly oxidized. The strain induced by the oxidation of the BZ gel is measured by recording its radius change when its catalyst concentration and its crosslinking density are varied independently. We choose the maximal radius during swelling as a metric of responsiveness of the hydrogel upon oxidation and assume this quantity to be the equilibrium size of the hydrogel when oxidized (Supplementary SM 4, SM 5). With this metric, the strain of a gel upon oxidation is shown to increase with catalyst concentration (Figure 2-a), while this strain decreases with increasing crosslinker density in the solution (Figure 2-b).

We interpret these experimental results in light of the Flory-Huggins equilibrium theory for polyelectrolyte gels [32]. In this model we conceptualize the gel as an entropic spring that balances the solvation forces generated by the polymer's interaction with water and the osmotic stress from the counterions. We imagine that the solvation and counterion pressures vary with the oxidation state of the catalyst of the BZ chemical reaction, but the properties of the entropic spring do not.

Specifically, we consider that the equilibrium size of a gel results from a balance between its entropic elasticity  $G_0(\frac{\Phi}{\Phi_0})^{\frac{1}{2}}$  and the sum of the osmotic pressure of the polymer  $\Pi_{\text{pol}} = \frac{k_{\text{B}}T}{\nu_v}(\frac{1}{2} - \chi)\Phi^2$  and of that of the counterions  $\Pi_{\text{ions}} = k_{\text{B}}T\frac{c_{\text{b}}}{4c_{\text{s}}}$ , with  $G_0$  the shear modulus of the gel in the reference state,  $\Phi_0$  the volume fraction of the gel in the reference state,  $\Phi$  the volume fraction of the gel,  $k_{\text{B}}$  the Boltzmann constant,  $T$  the temperature,  $\nu_v$  the volume of a solvent molecule or polymer, assumed to be the same here, and thus independent of the oxidative state of the ruthenium catalyst,  $\chi$  the adimensional parameter characterizing the interaction between the solvent and the polymer,  $c_{\text{b}}$  the number concentration of charges of the polymer and  $c_{\text{s}}$  the salt number concentration.

We derive two expressions for the elastic stress  $\Pi_{\text{elastic}}$  of a spherical gel of radius  $R$  as a function of its radial change  $\Delta R$  during oxidation of the ruthenium catalyst. The first one relates  $\Pi_{\text{elastic}}$  to the bulk modulus of the gel  $\kappa$  (Eqn. 1). The second one is deduced from the Flory-Huggins theory and states that  $\Pi_{\text{elastic}}$  is the sum of the change of counterions osmotic stress  $\Delta\Pi_{\text{ions}}$  and of the change of polymer osmotic stress  $\Delta\Pi_{\text{pol}}$  caused by the oxidation of the ruthenium catalyst (Eqn. 2,3,4) (Supplementary SM 9):

$$\Pi_{\text{elastic}} = 3\kappa\frac{\Delta R}{R} \quad (1)$$

$$\Pi_{\text{active}} = \Delta\Pi_{\text{ions}} + \Delta\Pi_{\text{pol}} \quad (2)$$

$$\Pi_{\text{active}} = k_{\text{B}}T\frac{5c_{\text{Ru}^{2+}}^2}{4c_{\text{s}}} + k_{\text{B}}T\frac{\Phi_{\text{red}}^2}{\nu_v}(\chi_{\text{red}} - \chi_{\text{ox}}) \quad (3)$$

$$\Pi_{\text{elastic}} = \Pi_{\text{active}} \quad (4)$$

with  $\Phi_{\text{red}}$  its volume fraction when the catalyst is in its reduced state,  $c_{\text{Ru}^{2+}}$  the concentration of ruthenium catalyst in the gel,  $\chi_{\text{red}}$  and  $\chi_{\text{ox}}$ , the  $\chi$  parameters of the polymer containing the reduced and oxidized form of the ruthenium catalyst, respectively.

We experimentally verified the relationship of Eqn. 1,  $\Pi_{\text{elastic}} = 3\kappa\frac{\Delta R}{R}$ , by varying  $\Pi_{\text{elastic}}$  using large molecular weight Dextran molecules of known concentration and tabulated osmotic pressure and measuring  $\frac{\Delta R}{R}$ . We observed a linear dependence between  $\Pi_{\text{elastic}}$  and  $\frac{\Delta R}{R}$  and deduced  $\kappa$  from the slope (see Materials and Methods)[38, 39]. For these experimental parameters, the gel behaves as an elastic spring.

To a first approximation, Eqn. 4 is consistent with the experimental observation that the swelling of the gel upon its oxidation is inversely proportional to its bulk modulus  $\kappa$  (Figure 2). Optimizing the strain can thus be simply achieved by making softer gels. This is an important result for the design of autonomous shape changing composite hydrogels, where a bending deformation can be induced by the differential swelling of two materials [18]. A well-known example of such a material is a bilayer, made from a swellable gel anchored to a thin rigid object. In this case, the deformation of the material, here a change of curvature, is solely controlled by its strain [21, 37].

### Optimizing the stress upon oxidation of BZ gels

By definition, the mechanical strain energy density is the product of the stress and strain. Therefore measuring the stress generated during the oxidation of different BZ gels is an important quantity to characterize and compare their chemomechanical energy performance. Moreover, note that the right hand side of Eqn. 3 does not depend on the bulk modulus  $\kappa$ , which is a passive elastic property of the gel. Thus measurements of stress ( $\Pi_{\text{elastic}}$ ) do not depend on  $\kappa$ , while measurements of strain alone, ( $\frac{\Delta R}{R}$ ), do. In other words, when a BZ gel experiences a large strain ( $\frac{\Delta R}{R}$ ) upon oxidation of the ruthenium catalyst, one can not distinguish if this is caused by a gel having a low bulk modulus or by a large active stress caused by the oxidation of the catalyst. Measuring  $\Pi_{\text{elastic}}$  allows one to disentangle the role of the chemical driving forces embodied by the terms involving solvation ( $\chi_{\text{red}} - \chi_{\text{ox}}$ ) and charged ions ( $\text{Ru}^{2+}$ ) from the elastic restorative forces characterized by  $\kappa$ .

We thus first examine the influence of the elasticity of the gel on the stress generated by the oxidation of the catalyst when the catalyst content is kept constant at 9mM. We observe that  $\Pi_{\text{elastic}}$  does not depend strongly on the elasticity of the gel and is limited to 30kPa (Figure 3-a). The softness of the gel increases both the strain

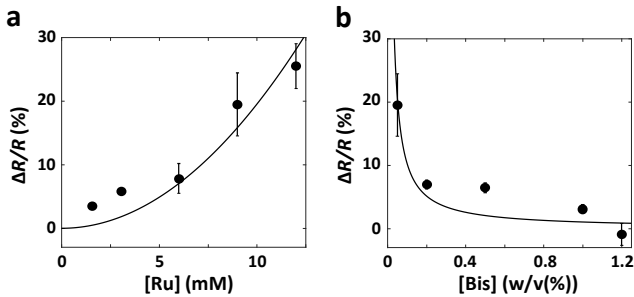


FIG. 2. (a) Relative maximal radius change  $\frac{\Delta R}{R}$  (%) as a function of catalyst concentration in mM for the concentration of the crosslinker in (w/v)(0.05%) in the pregel solution. The dash line represents the equation  $y \propto x^2$ . (b) Relative maximal radius change  $\frac{\Delta R}{R}$  (%) as a function of the concentration of the crosslinker in (w/v)(%) in the pregel solution for a catalyst concentration of 9mM. The bulk modulus is proportional to the cross-linker concentration (Supplementary SM 8). The dash line represents the equation  $y \propto \frac{1}{x}$ .

and the chemomechanical energy conversion, but does not increase much the stress generated by the oxidation of the catalyst.

We next study the influence of the gel's catalyst content on  $\Pi_{\text{elastic}}$ . The catalyst concentration is determined by measuring the absorbance of the gel (see Materials and Methods). We demonstrate that  $\Pi_{\text{elastic}}$  increases with the catalyst concentration for a concentration of up to 12mM (Figure 3-b). The stress, strain and the chemomechanical energy conversion generated by the oxidation of the BZ gel can therefore be engineered by tuning the catalyst concentration.

We now seek to quantify the role of the two chemical driving forces  $\Delta\Pi_{\text{pol}}$  and  $\Delta\Pi_{\text{ions}}$ . In all the analysis that follows, we compute  $\Delta\Pi_{\text{ions}} = k_B T \frac{5c_{\text{Ru}^{2+}}}{4c_s}$  from the measurements of  $c_{\text{Ru}^{2+}}$  and  $c_s$ . We assume the veracity of Eqn. 4,  $\Pi_{\text{elastic}} = \Delta\Pi_{\text{ions}} + \Delta\Pi_{\text{pol}}$ , and having measured  $\Pi_{\text{elastic}}$ , deduce the polymer osmotic stress,  $\Delta\Pi_{\text{pol}} = k_B T \frac{\Phi_{\text{red}}^2}{v_c} (\chi_{\text{red}} - \chi_{\text{ox}})$ , which is plotted in Figure 3-a for gels containing 9mM of catalyst. We observe a slight monotonic variation with the crosslinking concentration. For a gel with a bulk modulus of 10kPa,  $\Delta\Pi_{\text{pol}}$  increases with the catalyst concentration, as shown in Figure 3-b. More importantly, for the polymer under study, we determine that  $\Delta\Pi_{\text{pol}}$  is much larger than  $\Delta\Pi_{\text{ions}}$ , thus contributions to the measured elastic stress from the counterions is negligible compared to the change of solvation energy. This result yields insights into the mechanism responsible for the change of the  $\chi$  parameter of the gels. If one assumed that charges in the polymer gels interact via a repulsive Debye-Huckel electric potential, one can calculate the contribution of their electrostatic repulsions to the  $\chi$  parameter of the hydrogel. This theoretical argument predicts that an electrostatic osmotic stress  $\Pi_{\text{elec}}$  is generated by the electrostatic in-

teractions of the ruthenium catalyst when the ruthenium catalyst loses an electron and is equal to  $\Delta\Pi_{\text{ions}}$  in magnitude (Supplementary SM 9). However,  $\Delta\Pi_{\text{ions}}$  is much lower than the experimentally measured  $\Delta\Pi_{\text{pol}}$ . This proves that more complicated interactions than electrostatic repulsion, e.g. solvation forces, control the change of  $\chi$  parameter of the BZ gel.

There are also two additional measurements made on these gels which suggest interactions besides charge play a role in the gel chemomechanics. First, the bulk modulus of soft gels ( $\kappa \sim 10\text{kPa}$ ) increases linearly with the catalyst concentration (Supplementary SM 8). This observation demonstrates that the ruthenium monomer causes the polymer behavior to deviate from that of an ideal Gaussian polymer chain, as the elasticity of a crosslinked ideal Gaussian polymer chain is simply proportional to the concentration of crosslinker. The catalyst is thought to be connected to the polymer backbone as a pendant chain and therefore is not expected to affect the gel elasticity. Second, the equilibrium radius of the hydrogel decreases as the ruthenium catalyst content increases (Supplementary SM 10). This observation emphasizes the unexpected character of the ruthenium trisbipyridine molecule. A higher concentration of ruthenium catalyst in the gel is expected to both generate a higher concentration of counterions and a higher electrostatic repulsive interaction between ruthenium molecules. These effects should induce swelling of the gel, in stark contradiction with our experimental observations. Previous studies similarly highlight the importance of forces other than simple electrostatic interactions in the equilibrium properties of the gels. Indeed, BZ gels have been shown to shrink upon oxidation when multivalent ruthenium catalyst is used as a crosslinker, or when specific monomers compose the gels [22, 26–28]. Taken together, these observations spotlight the crucial role of the gel's molecular characteristics in its swelling behavior and the daunting challenge of explaining its thermodynamic equilibrium properties with entropy and electrostatic interactions as the only two physical effects.

Nonetheless, in the framework of the Flory-Huggins model, the effect of these additional molecular interactions on the macroscopic properties of BZ gels can be accounted for by introducing the  $\chi$  parameter. Therefore, we experimentally determine a quantitative estimate of the change of the  $\chi$  parameter of the gel during its oxidation,  $\delta\chi = \chi_{\text{red}} - \chi_{\text{ox}}$ , as a function of the catalyst and polymer concentration (Figure 3-c). To do so, we divide the osmotic stress generated by the polymer by the square of the density of the gel  $\rho$ . Estimations of gel's density as a function of the crosslinker concentration in solution and as a function of its catalyst concentration are respectively obtained by recording the free fall of the hydrogel in a water column and by measuring its relative change of equilibrium radius (Supplementary SM 10). For gels that have a catalyst concentration of  $\sim 9\text{mM}$ , we measure that  $\delta\chi$  is nearly constant with the polymer

concentration, ie the gel density (Inset-Figure 3-c). For gels that have a density of  $\sim 20\text{kg}\cdot\text{m}^{-3}$ , which corresponds to a concentration of polymer of 0.4M, we find that  $\delta\chi$  increases linearly with the catalyst concentration (Figure 3-c). Assuming that  $\delta\chi = \delta\chi_{Ru} \times p$  with  $p$  the fraction of ruthenium monomer to acrylamide monomer, we find that the order of magnitude of the energy change per molecules of ruthenium catalyst due to these molecular attractive interactions  $\delta\chi_{Ru}$  is around  $4k_B T$ .

As a conclusion to this part, we demonstrated that the strain generated during the oxidation of BZ gels can be tuned by increasing its catalyst concentration and decreasing its bulk modulus, an important result for the design of shape changing hydrogels. Additionally, we demonstrated that the stress (eq. 3) generated by BZ gels during the oxidation of the ruthenium catalyst is an appropriate metric for the assessment of actuation performance because the stress is directly related to the active chemical processes and does not depend on the passive bulk modulus of the gel, in contrast to the strain. Furthermore, the active stress upon oxidation of the gel is shown to be mainly controlled by solvation energy change, of entropic and/or enthalpic origins, captured by a change of the gel's  $\chi$  parameter.

### Influence of hydrogel size on BZ oscillatory chemistry

We next focus on optimizing the autonomous cyclic swelling of the BZ gel. For a BZ hydrogel to fully swell during each BZ chemical cycle, one needs to ensure that the swelling timescale of the gel is shorter than the time the gel stays in the oxidized and reduced state, subject to the additional constraint that the BZ reaction keeps oscillating. The swelling dynamics of a hydrogel follows a diffusion-like process consisting of the polymer network diffusing in a viscous solvent, with a characteristic time proportional to the square of the diameter of the gel [42]. Therefore, decreasing the radius of the BZ gel reduces its timescale of swelling. However, supporting chemical oscillation within gel beads requires that the rate of reaction producing chemicals inside the gel is faster than the rate of loss of those chemicals due to diffusion, a term that can depend on the gel's geometrical properties. In other words, nondimensional numbers made from the ratio of these two rates, e.g. Damköhler numbers,  $Da = \frac{\text{diffusion rate}}{\text{reaction rate}}$  predicts that gels oscillate when  $Da < 1$  [43].

We first investigate how the dynamics of the Belousov Zhabotinsky reaction is affected by the size of the BZ gel for various BZ solution composition, in particular the concentration of the oxidizer, sodium bromate. BZ beads of 3 different radii  $100\mu\text{m}$ ,  $220\mu\text{m}$  and  $285\mu\text{m}$  composed of 15%AAM, 1.5%AAc, 1% Bisacrylamide, functionalized with the ruthenium catalyst ( $c_{Ru^{2+}} \sim 10\text{mM}$ ) were immersed in a BZ solution containing  $[\text{H}_2\text{SO}_4]=0.6\text{M}$  sulfu-

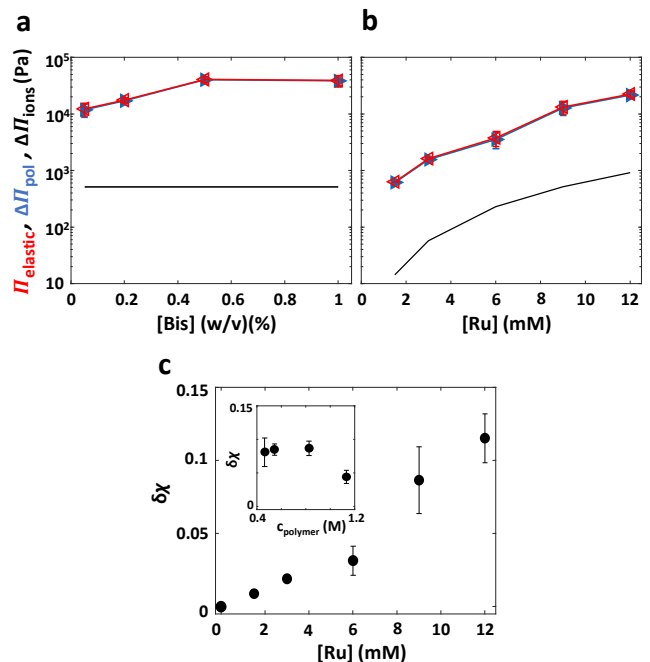


FIG. 3. The stresses defined in this figure are related as  $\Pi_{\text{elastic}} = \Delta\Pi_{\text{ions}} + \Delta\Pi_{\text{pol}}$ . (a) Elastic stress  $\Pi_{\text{elastic}}$  (red), osmotic stress of the polymer  $\Delta\Pi_{\text{pol}}$  (blue), expected osmotic stress of the counterions  $\Delta\Pi_{\text{ions}}$  (black) generated by the oxidation of the ruthenium catalyst as a function of crosslinker concentration in solution for gels with a catalyst concentration of 9mM. (b) Elastic stress  $\Pi_{\text{elastic}}$  (red), osmotic stress of the polymer  $\Delta\Pi_{\text{pol}}$  (blue), expected osmotic stress of the counterions  $\Delta\Pi_{\text{ions}}$  (black) generated by the oxidation of the ruthenium catalyst as a function of catalyst concentration for gels with a quantity of crosslinker in solution of 0.05%. (c)  $\delta\chi = \chi_{\text{red}} - \chi_{\text{ox}}$  as a function of the catalyst concentration in the BZ hydrogel. Inset:  $\delta\chi = \chi_{\text{red}} - \chi_{\text{ox}}$  as a function of the polymer concentration in the BZ hydrogel.

ric acid,  $[\text{MA}]=0.2\text{M}$  malonic acid,  $[\text{NaBr}]=0.1\text{M}$  sodium bromide, and sodium bromate of concentration varying from 0.16M to 0.42M. The change of color of the catalyst was recorded as a function of time (Figure 4-a). We observed that when the bromate concentration is below a critical threshold of  $c=0.24\text{M}$ , the gel does not chemically oscillate but rather remains in the reduced state (Figure 4-c). For gel beads of radius larger than  $200\mu\text{m}$ , the period of oscillation decreases as the bromate concentration increases. Moreover, we find that a gel of  $100\mu\text{m}$  radius never oscillates, even when the bromate concentration is increased (Figure 4-c). Therefore, we postulate that there exists a critical radius below which the gel does not oscillate.

To test our hypothesis, we construct a theoretical reaction-diffusion model in which the gel is coupled to its environment. We combine the Vanag-Epstein model for the BZ reaction kinetics with an additional loss term due to the efflux out of the gel of the mobile species  $[\text{Br}_2]$ ,  $[\text{Br}^-]$  and  $[\text{HBrO}_2]$  produced in the gel during the BZ reaction [44]. This loss term,  $-\alpha \frac{c_i}{R}$ , is proportional to

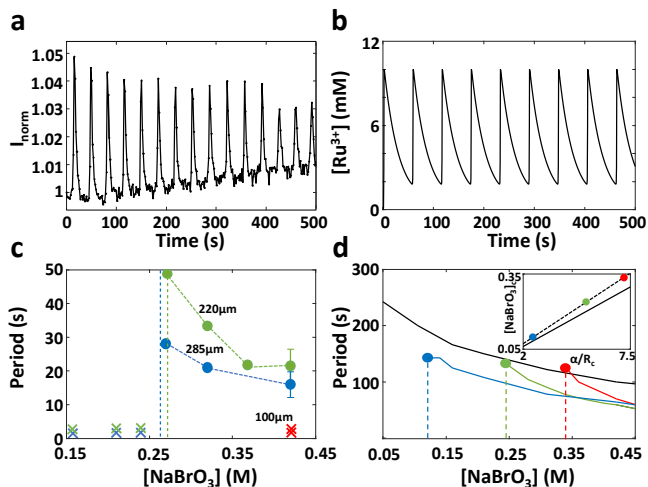


FIG. 4. (a) Intensity profile of a  $220\mu\text{m}$  radius BZ gel bead as a function of time in a BZ solution with a concentration of sodium bromate of  $0.42\text{M}$ . (b) The catalyst concentration as a function of time obtained from a Vanag Epstein model with a diffusive flux coefficient  $\frac{\alpha}{R} = 5\text{s}^{-1}$  and with a concentration of sodium bromate of  $0.42\text{M}$ . The model shows steady oscillation. (c) Experiment. Period of the BZ gel chemical oscillation as a function of the bromate concentration for different size of beads. Gels of  $100\mu\text{m}$ ,  $220\mu\text{m}$ ,  $285\mu\text{m}$  radius are represented respectively in red, green and blue. Disks and crosses represent chemically oscillating and non oscillating beads respectively. (d) Theory. Period of the BZ gel oscillation as a function of bromate concentration for various amplitudes of the diffusive flux  $\frac{\alpha}{R}$  obtained from the Vanag-Epstein model ( $\frac{\alpha}{R} = 7.15\text{s}^{-1}$ ,  $\frac{\alpha}{R} = 5\text{s}^{-1}$ ,  $\frac{\alpha}{R} = 2\text{s}^{-1}$ ,  $\frac{\alpha}{R} = 0\text{s}^{-1}$  are respectively represented in red, green, blue and black). Inset: Critical bromate concentration  $[\text{NaBrO}_3]_c$  as a function of the diffusive flux  $\frac{\alpha}{R_c}$  (Dashed line, numerical results; full line, theoretical prediction (Equation 2)).

the concentration of the species  $c_i$ , and inversely proportional to the radius of the bead  $R$  (see Materials and Methods)[43]. In agreement with our experimental observations, this theoretical model predicts that the period of oscillation decreases when the bromate concentration increases (Figure 4-d). The rate of change of the oscillation period increases when the size of the gel bead is smaller. Additionally, when the gel radius is below a critical threshold, the gel stops chemically oscillating and remains in the reduced state. The condition to observe oxidation of the beads simplifies to  $k_4 = 42 \times [\text{H}_2\text{SO}_4] \times [\text{NaBrO}_3] = 25.2 \times [\text{NaBrO}_3] > \frac{\alpha}{R}$  (equation 2) (Inset of Figure 4-d). This mathematical expression compares the production rate of the activator  $\text{HBrO}_2$  during the oxidation of the ruthenium catalyst with its loss rate due to its diffusion out of the gel bead. This model predicts that the critical size arises due to the loss of activator  $\text{HBrO}_2$  by diffusion and is consistent with experiment (Figure 4).

More precisely, the coupling via diffusion to the environment can be written as  $\alpha = \frac{D}{L}$  with  $D$  the diffusion coefficient of the chemicals, and  $L$  the scale over which

the chemical gradient is built.  $L$  can be controlled either by diffusion only or by diffusion and reaction, in case the chemical leaving the gel reacts in the media exterior to the gel. In the diffusion controlled case,  $L = R$ , whereas in the reaction-diffusion limited case,  $L = \sqrt{\frac{D}{k}}$ , with  $k$  the rate constant of consumption of the activator (SM 1-reaction A.2 of the Vanag-Epstein model with  $k_I = 2 \times 10^6 \text{M}\cdot\text{s}^{-1}$ ). The reaction-diffusion lengthscale is estimated to be smaller than the diffusion lengthscale for these experimental conditions, and we thus conclude that the outward flux of the activator is controlled by its reaction-diffusion property.

### The oscillatory strain of BZ gels is controlled by the timescale of gel swelling

Next, we measure the mechanical oscillations of such oscillating gels. Cyclic actuation of rigid gels as studied in Figure 4 is not detectable. Under the same chemical conditions, a softer gel ( $\kappa \sim 10\text{kPa}$ ) of  $230\mu\text{m}$  radius, just above the critical size for sustained chemical oscillation, displays a swelling amplitude of approximately 1% (Supplementary SM 11), one order of magnitude smaller than the relative radius change in oxidative solution.

To interpret this result, we measure the timescale of gel swelling by recording the radius of the gel as a function of time when an osmotic stress is applied. The experimental set up is identical to the one used to quantify the bulk modulus of the gel (Material and Methods). We measure that the swelling timescale is proportional to the square of the diameter of the gel (Supplementary SM 12). For the  $400\mu\text{m}$  diameter gel studied, the swelling timescale is around 100s. The oxidation spike is at most 10s. The expected volume change during the oxidation spike is then  $\frac{\Delta R_{\text{ox-BZ}}}{R_{\text{red-BZ}}} = \frac{\Delta R_{\text{ox}}}{R_{\text{red}}} (1 - \exp(-\frac{T_{\text{ox}}}{T_{\text{swelling}}})) \sim 2\%$ , in good agreement with the experimental value. The modest swelling amplitude in the oscillating BZ condition is caused by the slow timescale of gel swelling compared to the period of the BZ oscillation.

To further support this conclusion, we perform additional experiments with BZ gels that have longer periods of oscillation. The following composition of the BZ solution is used to lengthen transiently the period of the BZ gel chemical oscillations: ( $[\text{H}_2\text{SO}_4]=0.4\text{M}$ ,  $[\text{NaBrO}_3]=0.08\text{M}$ ,  $[\text{MA}]=0.06\text{M}$ ) [15, 21, 22, 26, 28, 29, 37] (Supplementary SM 13). We observe a significant cyclic volume change in the gels with a long period of oxidation and reduction. The magnitude of both the swelling and the shrinking amplitude of oscillating gels is now comparable to the strain obtained during their sole oxidation. An increase of the catalyst concentration and a decrease of the gel elasticity generates a larger strain, in agreement with the results obtained for experiments where the BZ gel is only oxidized. These results definitely prove that the discrepancy between the swelling timescale of the gel and the period of the BZ oscillation

is responsible for the modest actuation of the gel in the steady state regime. A straightforward solution to this limitation is to create porous BZ gels, where the chemical lengthscale is controlled by the size of the bead, and the swelling timescale is controlled by the size of the gel microstructure [23–25].

## CONCLUSION

We demonstrated a versatile two-step synthesis process of Belousov Zhabotinsky hydrogels that allows independent control of the BZ catalyst concentration, which is responsible for the active properties of the gel and the cross-linker concentration, which is primarily responsible for the passive gel elasticity. We observed that the swelling of BZ gels increases when increasing the catalyst concentration and when decreasing the cross-linker concentration, an important result for the design of autonomous shape-changing hydrogels.

Additionally, we introduced a new metric for assessing the chemomechanical energy conversion of active gels by quantifying their strain and their stress upon their oxidation. We argued that these two measurements are necessary to characterize the chemomechanical properties of a BZ oscillating gel. By definition, the mechanical strain energy density is the product of the stress and the strain. Moreover, we showed experimentally that the stress driving BZ gel swelling does not depend on the passive bulk modulus of the material. Thus, measuring the stress responsible for swelling the BZ gel allows separation of the contributions from the chemical driving forces and the restorative forces of the bulk modulus. These experimental results are supported by a Flory-Huggins model for polyelectrolytes, where we considered the source of the chemomechanics as arising from the hydration parameter  $\chi$  that varied with oxidation state of the BZ catalyst. We also deduced that interactions at the molecular level, which are more complex than simple electrostatic interactions, are responsible for the variation in the Flory-Huggins  $\chi$  parameter that occurs when the concentration of ruthenium incorporated in the gel is varied and when the ruthenium is oxidized.

Furthermore, we experimentally and theoretically studied how the radius of a spherical gel affects the period of the BZ reaction and controls even whether or not the gel oscillates. We measured the timescale of BZ gel swelling and demonstrated that the factor limiting the strain amplitude is the long swelling timescale of the gel compared to the shorter period of the BZ oscillation.

The methodology developed here of measuring both strain and stress in gels can be used to firstly, isolate the molecular composition of the BZ hydrogels that optimizes their chemomechanical energy conversion and secondly, design the shape and/or the microstructure of the gels that enhance the gel swelling timescale with respect to the period of the BZ reaction.

## MATERIALS AND METHODS

**Materials** Acrylamide (AAm) (99.9%), 1-ethyl-3-(3-(dimethylamino)propyl)carbodiimide HCl (EDC), N-hydroxysuccinimide (NHS), 2-(4-morpholino)ethanesulfonic acid (MES), hexadecane, 2-propanol, sodium phosphate monobasic anhydrous (99%), sodium phosphate dibasic anhydrous ( $\geq 99\%$ ), Tween 20, poly(dimethylsiloxane) (PDMS) elastomer kits (Sylgard 184) and sodium hydroxide (NaOH) were purchased from Thermo Fisher Scientific (Waltham, MA). Acrylic acid (AA) anhydrous (180-200ppm MEHQ inhibitor, 99%), 2-hydroxy-2-methylpropiophenone (Darocur 1173, photoinitiator), saline sodium citrate (SSC) buffer (20 $\times$  concentrate, molecular biology grade), N-Boc ethylene diamine, hydroxybenzotriazole (HOBt), N,N-dimethylformamide (DMF), Tetrahydrofuran (THF), N,N'-Diisopropylcarbodiimide (DIC) were purchased from Sigma-Aldrich (St. Louis, MO), N,N'-Methylenebis(acrylamide) (Bis) were purchased from Sigma Aldrich. 4-Methyl-4'-carboxy-2,2'-bipyridine was purchased from Carbosynth. All chemicals were of analytical grade and used without further purification.

**Micromolding-based fabrication of monodisperse polyacrylamide gels** The p(AAm-co-AA) microspheres in this study were fabricated according to methods in recent reports [36]. Briefly, the compositions of the aqueous prepolymer solutions were 15% (w/v) AAm, 0.5% to 10% (w/v) AAc, 0.05% to 1% (w/v) MBAM, and the composition of the wetting fluid was 99% (v/v) hexadecane and 1% (v/v) Darocur 1173 photoinitiator. As shown in Figure 1-a, the prepolymer solution was placed into a micropatterned PDMS mold, which was formed with Sylgard 184 containing 10% (w/w) curing agent following overnight incubation at 65 °C on a silicon master template. Bubbles in the microwells were removed by rubbing the surface of the mold with a disposable pipet tip. Excess prepolymer solution was removed via pipetting, and the wetting fluid was then placed on top of the mold in order to lead to surface tension-induced droplet formation. For beads with a diameter greater than 300 $\mu\text{m}$ , applying manually pressure around the hexagonal mold helps droplet formation. The mold was then carefully placed on an aluminum mirror (Thorlabs, Newton, NJ) and exposed to low-intensity 365 nm UV light with an 8 W hand-held UV lamp (Spectronics Corp., Westbury, NY) for 15 min to initiate radical chain polymerization. The microspheres were collected via pipetting, transferred to a microcentrifuge tube, and rinsed to remove any wetting fluid and unreacted chemicals as follows: mixing the microspheres in 2-propanol by pipetting, allowing them to settle to the bottom, and removing the supernatant. After rinsing at least three times with 2-propanol, the rinsing procedure was repeated at least three times with

deionized water containing 0.05% (v/v) Tween 20 and at least twice with 20 mM MES buffer (adjusted to pH 6 with 1 M NaOH) containing 0.05% (v/v) Tween 20 or deionized water.

**Catalyst synthesis** The ruthenium catalyst is synthesised in our lab with the following procedure. The starting material is commercially available 4-Methyl-4'-carboxy-2,2'-bipyridine from Carbosynth. The 4-Methyl-4'-carboxy-2,2'-bipyridine is further treated with an N-Boc ethylene diamine molecule to obtain the ligand N-(2-aminoethyl)-[2,2'-Bipyridine]-4-carboxamide. Then the catalyst is obtained by mixing this ligand in a 50 mL two-neck round-bottom flask connected to a condenser charged with dichloro(p-cymene)-ruthenium(II) dimer (100 mg, 0.163 mmol). We added 2 mL of distilled water and 18 mL of ethanol. Nitrogen was bubbled through the solution for 40 min. The mixture was distilled in darkness for 3 days. After the solvent was removed, the crude mixture was purified on a Sephadex-LH 20 column.

**Functionalizing the Hydrogel bead with the ruthenium catalyst via carbodiimide chemistry**

The second step of the fabrication process is to functionalize the hydrogel created above with a ruthenium catalyst complex. To do so, we use the reactivity of the carboxylic function with an amine group, to create an amide bond via EDC/NHS coupling. The carboxylate groups in the microspheres are first converted into reactive NHS ester groups. 400 mM EDC and 100 mM NHS are added to microspheres in 20 mM MES buffer (pH 6) containing 0.05% (v/v) Tween 20, mixed via pipetting, and placed on a rotator for 15 min at room temperature. Unreacted EDC and NHS are removed by rinsing the microspheres with 20 mM MES buffer (pH 6) containing 0.05% (v/v) Tween 20 at least three times and then 100mM sodium phosphate buffer adjusted to pH 8 by adding 1M of NaOH solution, at least twice. For ruthenium catalyst conjugation, p(AAm-co-AAc) microspheres activated with EDC/NHS (roughly 50 particles) are reacted with 10 $\mu$ L of a solution of 35mM ruthenium catalyst dissolved in DMF in 100 $\mu$ L of bead solution overnight on a rotator at room temperature in the sodium phosphate buffer adjusted to pH 8. Unreacted ruthenium BZ catalyst are removed by rinsing the microspheres 3 times with deionized water+0.05% (v/v) and at least 3 times with 5 $\times$ SSC buffer (pH 7) containing 0.05% (v/v) Tween 20. The BZ catalyst show good reactivity with the carboxylic function. We provide a proof of the covalent bonding between the carboxylic function and the amine group of the catalyst by doing a serie of test experiments either not using EDC, or NHS, or not using both of them. When washed with the same conditions, we observe that the BZ beads created under these test conditions do not show any color, proving that this washing procedure removes any unreacted catalyst.

The synthesized BZ gel bead (acrylamide, acrylic acid) do not show any non specific adsorption. Finally, we can check the homogeneity of the catalyst incorporation inside the gel bead, with a confocal microscope (SM 2).

**Experimental set up for characterizing the oscillating hydrogels**

Each experiment is conducted in a container made of a glass slide on the bottom and on the top, with a PDMS lateral wall of a few millimeters in height and a centimeter in diameter. The solution is kept under pressure with a clamp to avoid evaporation and the creation of carbon dioxide bubbles. The change of color of the catalyst is recorded as a function of time. Ruthenium-conjugated microspheres were visualized with an epifluorescence microscope (Olympus BX51 equipped with a DP70 microscope digital camera, Center Valley, PA) or a Leica S4 E Stereo Zoom Microscope with a MARLIN F-131C color camera. The images were then analyzed with the MATLAB software to obtain the temporal evolution of the intensity and the radius change of a gel.

**Details of the model**

The Vanag-Epstein (VE) model simplifies the BZ reaction to a model with only four variables, each representing a chemical concentration. The four concentration variables are  $c_1=[\text{HBrO}_2]$ ,  $c_2=[\text{Br}^-]$ ,  $c_3=[\text{oxidized catalyst}]=[\text{Ru}^{3+}]$  and  $c_4=[\text{Br}_2]$ .  $\text{HBrO}_2$ ,  $\text{Br}^-$  and  $\text{Br}_2$  are chemicals which can diffuse out of the gel, whereas the  $\text{Ru}^{3+}$  is bound to the gel. The mathematical expression of the loss term can be justified as follows [43]. Consider the number of moles of a chemical product inside the bead  $N_{i,in}$ . This product is diffusing out of the gel with a flux  $j$  proportional to its concentration,  $j = \alpha' c$ . The variation of the number of moles of product inside the bead  $dN_{i,in}$  due to diffusion can be written:

$$\frac{dN_{i,in}}{dt} = -j\pi R^2$$

$$\frac{d(\frac{4}{3}\pi R^3 c_i)}{dt} = -\alpha' \pi c_i R^2$$

The size of a rigid bead is constant, so the temporal variation of the concentration of this product takes the following form:

$$\frac{dc_i}{dt} = -\frac{3\alpha'}{4R} c_i$$

The diffusion acts then as an additional effective first order chemical reaction on the temporal evolution of the

chemical concentration. We define  $\alpha = \frac{3\alpha'}{4}$ .

$$\begin{aligned}\frac{dc_1}{dt} &= -k_1c_1c_2 + k_2c_2 - 2k_3c_1^2 + k_4c_1 \frac{(c_{3,0} - c_3)}{c_{3,0} - c_3 + c_{min}} \\ &\quad - \frac{\alpha}{R}c_1 \\ \frac{dc_2}{dt} &= -3k_1c_1c_2 - 2k_2c_2 - k_3c_1^2 + k_7c_4 + k_9c_3 - \frac{\alpha}{R}c_2 \\ \frac{dc_3}{dt} &= 2k_4c_1 \frac{(c_{3,0} - c_3)}{c_{3,0} - c_3 + c_{min}} - k_9c_3 - k_{10}c_3 \\ \frac{dc_4}{dt} &= 2k_1c_1c_2 + k_2c_2 + k_3c_1^2 - k_7c_4 - \frac{\alpha}{R}c_4\end{aligned}$$

The rate constant of reaction  $k_i$  and the constant concentration  $c_{min}$  are given in the supplementary material (SM 1).

We solve this coupled non linear differential equation using the MATLAB solver ode45.

**Measuring the catalyst concentration** The catalyst concentration is measured by squeezing the gel into a flat slab between two glass plate separated by a gap of known thickness, created by a double sticky tape. In parallel, a microfluidic chamber of the same thickness with a scale of known concentration of catalyst in solution is created. We measure the transmitted light  $I$  through the sample, for the same light condition for the BZ bead and the solution. The liquid sample of known concentration enables us to convert the transmitted light intensity into real concentration value, via a fitting function in agreement with a Beer Lambert Law (SM 3).

**Measuring the Bulk modulus by applying an osmotic stress with high molecular weight polymer Dextran** To achieve this measurement, we design a microfluidic chamber made of double sticky tape of thickness  $500\mu\text{m}$  and drill a hole of 1mm diameter and  $500\mu\text{m}$  height on a Plexiglas sheet. We flow successively solutions of sulfuric acid at a concentration of 0.4M with different Dextran concentration. We use a high molecular weight Dextran (MW=500 000g.mol<sup>-1</sup>, MW=2 000 000g.mol<sup>-1</sup>), to avoid the molecule diffusing inside the hydrogel. We measure the radius of the gel at mechanical equilibrium for each dextran concentration. The osmotic stress  $\Pi_{dex}$  is given by:

$$\log_{10}[\Pi_{dex}(w)] = 1.75 + 1.03w^{0.383} \quad (5)$$

with  $w$  the weight pourcent of Dextran in the solution [45, 46].

**Timescale of gel swelling** To achieve this measurement, we design a microfluidic chamber made of double sticky tape of thickness  $500\mu\text{m}$  and drill a hole of 1mm diameter and  $500\mu\text{m}$  height on a Plexiglas sheet. We flow successively solutions of sulfuric acid

at a concentration of 0.4M with a concentration of 5% Dextran concentration. We use a high molecular weight Dextran (MW=500 000g.mol<sup>-1</sup>, MW=2 000 000g.mol<sup>-1</sup>), to avoid the molecule diffusing inside the hydrogel. We record the evolution of the diameter of the gel  $D$  as a function of time. We then fit these data with an exponential function having a characteristic time  $\tau$ . We finally verify that the characteristic time of swelling  $\tau$  is proportional to the square of the gel diameter  $D$  (SM 12).

**Measuring the density** To measure the density of micrometric hydrogels, we determine their steady state velocity during their free fall in a water column  $V_\infty$ . The water column is a plastic cuvette used for absorbance measurement graduated every 5mm.

$V_\infty$  is directly related to the difference of density between the surrounding medium and the object.

$$\Delta\rho = \rho_g - \rho_w = \frac{9}{2} \frac{\eta V_\infty}{gR^2} \quad \text{with } \Delta\rho = \rho_g - \rho_w \quad (6)$$

with  $\Delta\rho$ ,  $\eta$ ,  $R$ ,  $V_\infty$  being, g respectively the difference of density between the hydrogel  $\rho_g$  and the water  $\rho_w$ , the dynamic viscosity of water, the radius of the bead, the velocity of the beads in the steady regime and the gravitational acceleration on Earth. Additional information are presented in the supplementary materials (SM 10).

## DATA AVAILABILITY

All data generated for this study are included in the main and supplementary figures. Other data that support the findings of this study are available on reasonable request from the corresponding author.

## ACKNOWLEDGMENT

We thank A.Agvhami for help with confocal imaging, B.Xu for sharing chemical tools, I.Dellatolas for critical reading of the manuscript and D.Blanc for help with the figures. We acknowledge useful discussions with M.M.Norton, G.Duclos, B.Rogers, R.Hayward, H.Kim, T.Emrick and I.Epstein.

## AUTHORS CONTRIBUTION

B.B., Z.Z., S.F devised the experiments. B.B., E.L., H.Y. fabricated the gels, N.Z., B.B synthesized the ruthenium catalyst, B.B developed the models, B.B, S.F. wrote the manuscript. The experiments were done at Brandeis University and mainly supported by NSF DMR-1534890. B.B acknowledges support of the Brandeis Provost research award. E.L., H.Y. gratefully acknowledge financial support by U.S. National Science

Foundation (grant NSF CBET-1703547). The authors declare no competing interests.

- 
- [1] Litschel, T., Ramm, B., Maas, R., Heymann, M., & Schwille, P. (2018). Beating vesicles: encapsulated protein oscillations cause dynamic membrane deformations. *Angewandte Chemie International Edition*, 57(50), 16286-16290.
- [2] Shastri, A., McGregor, L. M., Liu, Y., Harris, V., Nan, H., Mujica, M., ... & He, X. (2015). An aptamer functionalized chemomechanically modulated biomolecule catch-and-release system. *Nature chemistry*, 7(5), 447-454.
- [3] Thubagere, A. J., Li, W., Johnson, R. F., Chen, Z., Doroudi, S., Lee, Y. L., ... & Qian, L. (2017). A cargo-sorting DNA robot. *Science*, 357(6356).
- [4] Wu, K. T., Hishamunda, J. B., Chen, D. T., DeCamp, S. J., Chang, Y. W., Fernández-Nieves, A., ... & Dogic, Z. (2017). Transition from turbulent to coherent flows in confined three-dimensional active fluids. *Science*, 355(6331).
- [5] Merindol, R., & Walther, A. (2017). Materials learning from life: concepts for active, adaptive and autonomous molecular systems. *Chemical Society Reviews*, 46(18), 5588-5619.
- [6] Needleman, D., & Dogic, Z. (2017). Active matter at the interface between materials science and cell biology. *Nature Reviews Materials*, 2(9), 1-14.
- [7] Lee, K. Y., Park, S. J., Lee, K. A., Kim, S. H., Kim, H., Meroz, Y., ... & Shin, K. (2018). Photosynthetic artificial organelles sustain and control ATP-dependent reactions in a protocellular system. *Nature biotechnology*, 36(6), 530-535.
- [8] Ricotti, L., Trimmer, B., Feinberg, A. W., Raman, R., Parker, K. K., Bashir, R., ... & Menciassi, A. (2017). Biohybrid actuators for robotics: A review of devices actuated by living cells. *Science Robotics*, 2(12).
- [9] Park, S. J., Gazzola, M., Park, K. S., Park, S., Di Santo, V., Blevins, E. L., ... & Parker, K. K. (2016). Phototactic guidance of a tissue-engineered soft-robotic ray. *Science*, 353(6295), 158-162.
- [10] Wang, Wei and Lv, Xianglong and Moran, Jeffrey L. and Duan, Shifang and Zhou, Chao. (2020). A practical guide to active colloids: choosing synthetic model systems for soft matter physics research. *Soft Matter*, 16, 3846-3868.
- [11] Wehner, M., Truby, R. L., Fitzgerald, D. J., Mosadegh, B., Whitesides, G. M., Lewis, J. A., & Wood, R. J. (2016). An integrated design and fabrication strategy for entirely soft, autonomous robots. *Nature*, 536(7617), 451-455.
- [12] Christianson, C., Goldberg, N. N., Deheyn, D. D., Cai, S., & Tolley, M. T. (2018). Translucent soft robots driven by frameless fluid electrode dielectric elastomer actuators. *Science Robotics*, 3(17).
- [13] Shin, B., Ha, J., Lee, M., Park, K., Park, G. H., Choi, T. H., ... & Kim, H. Y. (2018). Hygrobot: A self-locomotive ratcheted actuator powered by environmental humidity. *Science Robotics*, 3(14).
- [14] Lancia, F., Ryabchun, A., & Katsonis, N. (2019). Life-like motion driven by artificial molecular machines. *Nature Reviews Chemistry*, 3(9), 536-551.
- [15] Yoshida, R., Takahashi, T., Yamaguchi, T., & Ichijo, H. (1996). Self-oscillating gel. *Journal of the American Chemical Society*, 118(21), 5134-5135.
- [16] A. M. Zhabotinsky, *Dokl. Akad. Nauk SSSR*, 1964, 157, 392.
- [17] R. M. Noyes, R. Field and E. Koros, *J. Am. Chem. Soc.*, 1972, 94, 1394-1395.
- [18] Na, J. H., Evans, A. A., Bae, J., Chiappelli, M. C., Santangelo, C. D., Lang, R. J., Hull, T.C., & Hayward, R. C. (2015). Programming reversibly self-folding origami with micropatterned photo-crosslinkable polymer trilayers. *Advanced Materials*, 27(1), 79-85.
- [19] Levin, I., Deegan, R., & Sharon, E. (2020). Self-oscillating membranes: Chemomechanical sheets show autonomous periodic shape transformation. *Physical Review Letters*, 125(17), 178001.
- [20] Li, S., Matoz-Fernandez, D. A., Aggarwal, A., & de la Cruz, M. O. (2021). Chemically controlled pattern formation in self-oscillating elastic shells. *Proceedings of the National Academy of Sciences*, 118(10).
- [21] Maeda, S., Hara, Y., Sakai, T., Yoshida, R., & Hashimoto, S. (2007). Self-walking gel. *Advanced Materials*, 19(21), 3480-3484.
- [22] Aizenberg, M., Okeyoshi, K., & Aizenberg, J. (2018). Inverting the Swelling Trends in Modular Self-Oscillating Gels Crosslinked by Redox-Active Metal Bipyridine Complexes. *Advanced Functional Materials*, 28(27), 1704205.
- [23] Takeoka, Yukikazu, Masayoshi Watanabe, and Ryo Yoshida. "Self-sustaining peristaltic motion on the surface of a porous gel." *Journal of the American Chemical Society* 125.44 (2003): 13320-13321.
- [24] Suzuki, Daisuke, Takeshi Kobayashi, Ryo Yoshida, and Toshihiro Hirai. "Soft actuators of organized self-oscillating microgels." *Soft Matter* 8, no. 45 (2012): 11447-11449.
- [25] Hu, Y., & Pérez-Mercader, J. (2017). Controlled Synthesis of Uniform, Micrometer-Sized Ruthenium-Functionalized Poly (N-Isopropylacrylamide) Gel Particles and their Application to the Catalysis of the Belousov-Zhabotinsky Reaction. *Macromolecular rapid communications*, 38(3), 1600577.
- [26] Zhang, Ye, et al. "Active Cross-Linkers that Lead to Active Gels." *Angewandte Chemie International Edition* 52.44 (2013): 11494-11498.
- [27] Yuan, P., Kuksenok, O., Gross, D. E., Balazs, A. C., Moore, J. S., & Nuzzo, R. G. (2013). UV patternable thin film chemistry for shape and functionally versatile self-oscillating gels. *Soft Matter*, 9(4), 1231-1243.
- [28] Kramb, R. C., Buskohl, P. R., Dalton, M. J., & Vaia, R. A. (2015). Belousov-Zhabotinsky hydrogels: Relationship between hydrogel structure and mechanical response. *Chemistry of Materials*, 27(16), 5782-5790.
- [29] Chen, I. C., Kuksenok, O., Yashin, V. V., Moslin, R. M., Balazs, A. C., & Van Vliet, K. J. (2011). Shape-and size-dependent patterns in self-oscillating polymer gels. *Soft Matter*, 7(7), 3141-3146.
- [30] Buskohl, P. R., & Vaia, R. A. (2016). Belousov-Zhabotinsky autonomic hydrogel composites: Regulating waves via asymmetry. *Science advances*, 2(9), e1600813.
- [31] Hara, Y., Mayama, H., & Morishima, K. (2014). Generative force of self-oscillating gel. *The Journal of Physical Chemistry B*, 118(9), 2576-2581.
- [32] Doi, M. (2013). *Soft matter physics*. Oxford University Press.
- [33] Masuda, T., Terasaki, A., Akimoto, A. M., Nagase, K., Okano, T., & Yoshida, R. (2015). Control of

- swelling–deswelling behavior of a self-oscillating gel by designing the chemical structure. *RSC Advances*, 5(8), 5781-5787.
- [34] Smith, M. L., Heitfeld, K., Slone, C., & Vaia, R. A. (2012). Autonomic hydrogels through postfunctionalization of gelatin. *Chemistry of Materials*, 24(15), 3074-3080.
- [35] Kramb, R. C., Buskohl, P. R., Slone, C., Smith, M. L., & Vaia, R. A. (2014). Autonomic composite hydrogels by reactive printing: materials and oscillatory response. *Soft matter*, 10(9), 1329-1336.
- [36] Liu, E. Y., Jung, S., & Yi, H. (2016). Improved protein conjugation with uniform, macroporous poly (acrylamide-co-acrylic acid) hydrogel microspheres via EDC/NHS chemistry. *Langmuir*, 32(42), 11043-11054.
- [37] Smith, M. L., Slone, C., Heitfeld, K., & Vaia, R. A. (2013). Designed autonomic motion in heterogeneous Belousov–Zhabotinsky (BZ)-gelatin composites by synchronicity. *Advanced Functional Materials*, 23(22), 2835-2842.
- [38] Dolega, M. E., Delarue, M., Ingremeau, F., Prost, J., Delon, A., & Cappello, G. (2017). Cell-like pressure sensors reveal increase of mechanical stress towards the core of multicellular spheroids under compression. *Nature communications*, 8, 14056.
- [39] Bonnet-Gonnet, C., Belloni, L., & Cabane, B. (1994). Osmotic pressure of latex dispersions. *Langmuir*, 10(11), 4012-4021.
- [40] Jia, D., & Muthukumar, M. (2019). Interplay between Microscopic and Macroscopic Properties of Charged Hydrogels. *Macromolecules*.
- [41] Zhang, Y., Zhang, B. , Kuang, Y. , Gao, Y., Shi, J. , Zhang, X.X. & Xu, B. A Redox Responsive, Fluorescent Supramolecular Metallohydrogel Consists of Nanofibers with Single-Molecule Width. *Journal of the American Chemical Society* 2013 135 (13), 5008-5011
- [42] Doi, M. (2009). Gel dynamics. *Journal of the Physical Society of Japan*, 78(5), 052001.
- [43] Yoshikawa, K., Aihara, R., & Agladze, K. (1998). Size-Dependent Belousov-Zhabotinsky Oscillation in Small Beads. *The Journal of Physical Chemistry A*, 102(39), 7649-7652.
- [44] Vanag, V. K., & Epstein, I. R. (2009). A model for jumping and bubble waves in the Belousov–Zhabotinsky-aerosol OT system. *The Journal of Chemical Physics*, 131(10), 104512.
- [45] Parsegian, V.A., Rand, R.P., Fuller, N.L., & Rau, D.C. (1986). [29] Osmotic stress for the direct measurement of intermolecular forces. *Methods in Enzymology*, Academic Press, 127, 400-416.
- [46] Monnier, S., Delarue, M., Brunel, B., Dolega, M. E., Delon, A., & Cappello, G. (2016). Effect of an osmotic stress on multicellular aggregates. *Methods*, 94, 114-119.